THE JOURNAL OF BIOLOGICAL CHEMISTRY
Vol. 279, No. 22, Issue of May 28, pp. 23061–23072, 2004
Printed in U.S.A.

pH and Cation-induced Thermodynamic Stability of Human Hyaluronan Binding Protein 1 Regulates Its Hyaluronan Affinity*

Received for publication, September 26, 2003, and in revised form, February 6, 2004
Published, JBC Papers in Press, March 5, 2004, DOI 10.1074/jbc.M310676200

Babal Kant Jha‡, Nivedita Mitra§, Rachita Rana‡ Avadhesha Surolia§, Dinakar M. Salunke¶, and Kasturi Datta‡‖**

From ‡103 Biochemistry Laboratory, School of Environmental Sciences, Jawaharlal Nehru University, New Delhi 110 067, India, the §Molecular Biophysics Unit, Indian Institute of Science, Bangalore 560012, Karnataka, India, the ¶Structural Biology Unit, National Institute of Immunology, Aruna Asaf Ali Marg, New Delhi 110 067, India, and the ‖Special Centre for Molecular Medicine, Jawaharlal Nehru University, New Delhi-110 067, India

Hyaluronan-binding protein 1 (HABP1) is a trimeric protein with high negative charges distributed asymmetrically along the faces of the molecule. Recently, we have reported that HABP1 exhibits a high degree of structural flexibility, which can be perturbed by ions under *in vitro* conditions near physiological pH (Jha, B. K., Salunke, D. M., and Datta, K. (2003) *J. Biol. Chem.* 278, 27464–27472). Here, we report the effect of ionic strength and pH on thermodynamic stability of HABP1. Trimeric HABP1 was shown to unfold reversibly upon dissociation ruling out the possibility of existence of folded monomer. An increase in ionic concentration (0.05–1 M) or decrease in pH (pH 8.0–pH 5.0) induced an unusually high thermodynamic stability of HABP1 as reflected in the gradual increase in transition midpoint temperature, enthalpy of transition, and conformational entropy. Our studies suggest that the presence of counter ions in the molecular environment of HABP1 leads to dramatic reduction of the intramolecular electrostatic repulsion either by de-ionizing the charged amino acid residues or by direct binding leading to a more stable conformation. A regulation on cellular HA-HABP1 interaction by changes in pH and ionic strength may exist, because the more stable conformation attained at higher ionic strength or at acidic pH showed maximum affinity toward HA as probed either in solid phase binding assay on HA-immobilized plates or an in-solution binding assay using intrinsic fluorescence of HABP1.

The diverse biological roles of hyaluronan, a complex polysaccharide in vertebrates, are now established beyond any doubt. These include acting as a vital structural component of connective tissues, the formation of loose hydrated matrices that allow cells to divide and migrate during development, and in intracellular signaling (1–5). Such variable activities may result from its interaction with a family of proteins known as hyaladherin (2).

Hyaluronan-binding protein 1 (HABP1),[1] one of the members of hyaladherin family was identified (6) and its role in different cellular processes like cell adhesion and tumor invasion, sperm maturation, and motility (7–11) are under intensive investigation in our laboratories. Molecular cloning of human HABP1 revealed its multifunctional nature as its sequence was found to be identical with p32, a protein co-purified with splicing factor SF2 and with the receptor of the globular head of complement factor C1q (gC1qR). It is represented as synonyms of p32/C1QBP (accession number NP_001203) in human chromosome 17. This molecule has generated a considerable interest in the last few years largely because of its multifarious functions as well as its localization in various subcellular compartments including cell surface in different cell types (8–17). However, only one transcript of HABP1 was detected from different types of tissues suggesting that no other isoform(s) of HABP1 exist in different cell types (16).

Studies on the crystal structure of p32/HABP1 revealed that it exists as a homotrimer, and each protomer consists of seven consecutive twisted anti-parallel β-sheets flanked by one NH_2-terminal and two COOH-terminal α-helices and that the terminal α-helices have extensive intra- as well as intermolecular contacts. It has been postulated that these terminal helices are critical for maintaining the trimeric assembly and protein-protein interactions (18). In a previous report, we have shown that HABP1 exists predominantly as a non-covalently linked trimer near physiological conditions and as a hexamer (dimer of trimers) in the oxidative environment (19). Being acidic in nature and having highly polar amino acid residues distributed asymmetrically on the surface, the electrostatic interactions in HABP1 are expected to have a role in dictating its folding topology and tertiary interactions. However, the relative role of the contribution of electrostatic interactions to protein stability, compared with that of hydrophobic interactions, has been the subject of long standing query (20). Part of the difficulty, in discriminating the contributions from electrostatic effect, stems from the fact that there are several different ways in which they contribute to the net stability of the native conformation. In addition, both attractive and repulsive electrostatic interactions are possible. In general, models to account for co-solute effects on protein stability may be classified in a number of ways; two major classifications are those in which the co-solute directly interacts with the protein, *i.e.* binding, or

* This work was supported by Department of Biotechnology, Government of India Grant BT/PR2053/BRB/15/197/2000 to the School of Environmental Sciences, Jawaharlal Nehru University. VP-DSC is provided at the Molecular Biophysics Unit by the Department of Science and Technology under the Intensification of Research in High Priority Areas. The costs of publication of this article were defrayed in part by the payment of page charges. This article must therefore be hereby marked "*advertisement*" in accordance with 18 U.S.C. Section 1734 solely to indicate this fact.

** To whom correspondence should be addressed: 103 Biochemistry Laboratory, SES, Jawaharlal Nehru University, New Delhi 110 067, India. Tel.: 91-11-26704327 or 26717538; Fax: 91-11-26717502; E-mail: kdatta@mail.jnu.ac.in.

[1] The abbreviations used are: HABP1, Hyaluronan-binding protein 1; MES, 4-morpholineethanesulfonic acid; ABTS, 2,2′-azinobis(3-ethylbenzthiazoline-6-sulfonic acid); HRP, horseradish peroxidase; ASA, accessible surface areas; DSC, differential scanning calorimetric; HA, hyaluronan.

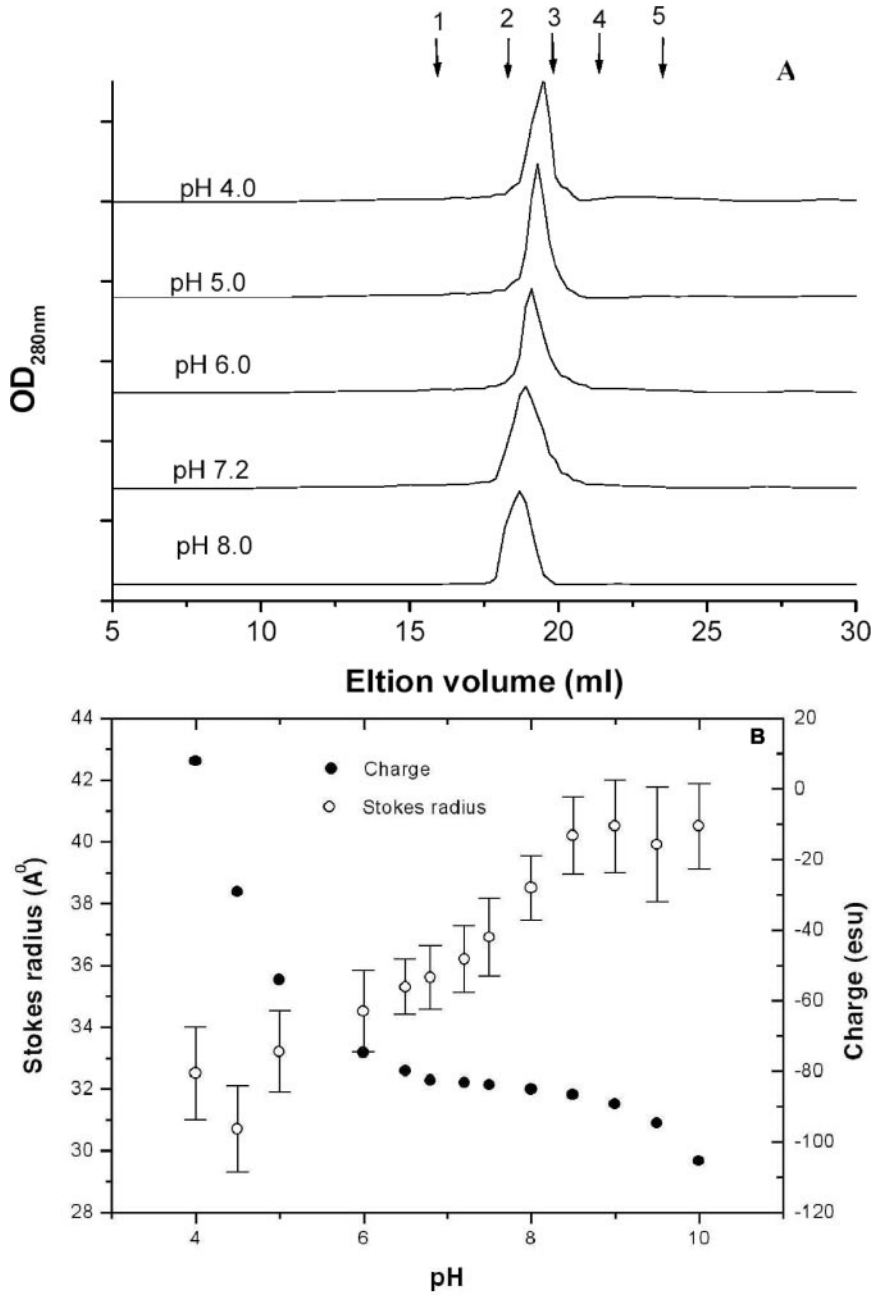

FIG. 1. **pH induced changes in hydrodynamic properties of trimeric HABP1.** *A*, 100 μl of 1 mg/ml HABP1 in 10 mM buffer at different pH values (phosphate, pH 6.5–8; MES, pH 5.5–6.3; and acetate, pH 4.0–5.5) and at constant ionic strength (150 mM) were injected on a Superose-6 HR30 analytical column at a elution speed of 0.3 ml/min. The mean elution volume of HABP1 at different pH values was plotted against the optical density at 280 nm. The column calibrated with standard molecular mass markers of different Stokes radii, alcohol dehydrogenase (*1*) (150 kDa, 46 Å), bovine serum albumin (*2*) (67 kDa, 35.5 Å), ovalbumin (*3*) (43 kDa, 30.5 Å), chymotrypsinogen (*4*) (25 kDa, 20.9 Å), and ribonuclease A (*5*) (13.7 kDa, 16.4 Å), were determined. *B*, the Stokes radii of HABP1 under different conditions of pH were calculated as described under "Materials and Methods" and plotted against pH along with the charges on HABP1 at different pH values as calculated using ANTHEPROT. The S.D. ($n = 3$) is shown as ($\pm$) *error bars* on each data point.

those involving effects on the solvent, *e.g.* excluded volume effects (21). Previously, we have shown that HABP1 exists in an expanded molten globule-like state at low ionic strength around alkaline pH because of charge-charge repulsion emanating from the presence of multiple negatively charged carboxyl groups, and that the addition of low concentrations of cations leads to a substantial compaction of HABP1 (22). The effect of cation is attributed to their minimizing the charge repulsion by binding to the negatively charged groups, which in turn diminish the repulsive interaction (23). Similar effects, in cases involving the presence of anions, appear to result in the refolding of intrinsically disordered protein that have a net positive charge at neutral pH (24).

In terms of the overall spectrum of protein stability ranging from intrinsically unstructured protein at one extreme to very stable, globular proteins at the other, HABP1 is in the middle. In other words, there are many other proteins that may have marginal or even lower stability under physiological conditions. Thus, the effects of salts and pH on HABP1 are likely to be applicable to a number of other eukaryotic proteins, and to further our understanding of the broad range of interactions of ions with proteins. Recently, we have reported the structural flexibility of HABP1 under a wide range of ionic environments. At low ionic strength HABP1 exists in highly expanded and loosely held trimeric structures, whereas, the presence of salt induces compact trimeric structure (22). Thus the possibility of minimizing the intramolecular repulsion by counter ions leading to stable conformation needs to be examined. Also being an oligomeric protein, the studies on HABP1 can provide important insights into the relative contributions of the various forces under different conditions of pH, ion concentration, and temperature that stabilize the oligomeric structures of proteins in various stable or meta-stable conformations.

MATERIALS AND METHODS

EAH-Sepharose 4B, all empty XK, pre-packed Resource-Q, and Superose-6 HR10/30 columns and the gel filtration calibration kit were from Amersham Biosciences. All other chemicals (unless otherwise mentioned) were of the highest purity grade available and obtained

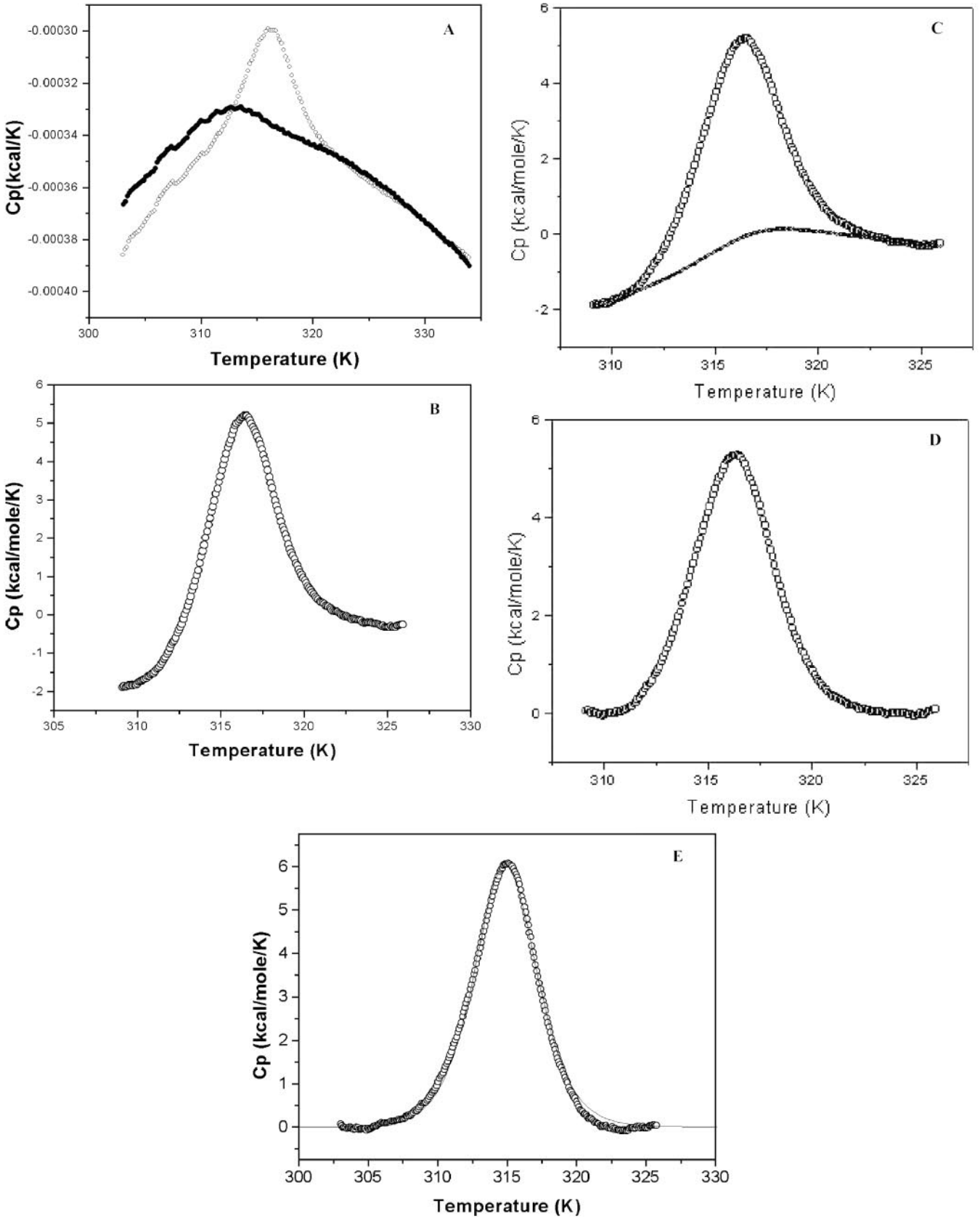

FIG. 2. **Ultrasensitive DSC scan of HABP1.** 14 μM in trimer equivalent of HABP1 in 10 mM phosphate buffer containing 200 mM NaCl, pH 7.2, at a scan rate of 20 K h^{-1}. Graphic illustration of the fitting procedure used. *A*, raw DSC data for calorimetric transition of HABP1 (*open circle*) compared with buffer alone. Scan was obtained with buffer in both sample and reference cells of the calorimeter (*solid circle*). *B*, buffer/buffer baseline-subtracted concentration-normalized (14 μM) raw data for the scan are shown in *a*. *C*, progress baseline connection (*solid circle*) of pre- and post-transition baselines of the raw data (*open circle*) are shown in *c*. *D*, progress baseline-subtracted DSC data used for fitting. *E*, final fitted calorimetric scan. The data points are shown as *open circles* and a two-state fit is depicted as *solid lines*. The fitting was done using Origin 5.0.

from Sigma and highly purified HA-octasaccharide was a generous gift from Dr. Akira Asari of Seikagaku Corp., Japan. Milli-Q™ grade water was used for preparing all the solutions required for the study. Urea was purchased from Sigma and further purified by re-crystallization before use.

Purification and Concentration Determination of HABP1—Recombinant HABP1 was produced in *Escherichia coli* as described earlier (7). The protein was purified by a 65–90% ammonium sulfate fractionation, followed by ion exchange chromatography on a Resource-Q (6 ml) column (Amersham Biosciences), interfaced with a Pharmacia FPLC™ system (Amersham Biosciences) using a linear gradient of 0–1 M NaCl in 20 mM HEPES, 1 mM EDTA, 1 mM EGTA, 5% glycerol, and 0.2% 2-mercaptoehanol, pH 7.5, followed by hyaluronan-Sepharose affinity column chromatography as reported earlier (19, 22). Affinity purified HABP1 was further purified by size exclusion chromatography as described earlier (19). For all practical purposes the concentration of a known aliquot was determined in 20 mM phosphate buffer, pH 6.5, containing 6 M guanidine-HCl by measuring the absorbance at 280 nm at 25 °C on a Cary 100 Bio UV visible double beam spectrophotometer (Varian Inc., Mulgrave, Australia) interfaced with a Peltier thermal controller. The molar extinction coefficient of denatured HABP1 was calculated and found to be 22,190 at 280 nm, which corresponds to $A^{0.1\%}_{280\ nm} = 0.932$ (22).

Gel Permeation Chromatography—Gel permeation chromatography of HABP1 was carried out on a Pharmacia Superose-6™ HR10 × 30 analytical column interfaced with Pharmacia FPLC™ system at a constant flow rate of 0.3 ml/min. The buffer concentration used was 10 mM: phosphate, pH 6.5–8; MES, pH 5.5–6.3; acetate, pH 4.0–5.4; and citrate phosphate, pH 3.0–4.4, keeping the ionic concentration constant at 150 mM using NaCl at all pH values. The standard molecular mass markers of known molecular mass and Stokes radii: alcohol dehydrogenase (150 kDa, 46 Å): bovine serum albumin (67 kDa, 35.5 Å), ovalbumin (43 kDa, 30.5 Å), chymotrypsinogen (25 kDa, 20.9 Å), and ribonuclease A (13.7 kDa, 16.4 Å), were independently run to calibrate the column prior to sample run. Stokes radii were determined from a plot of Stokes radius *versus* K_{av}, where K_{av} is defined as $(V_e - V_o)/(V_t - V_o)$, where V_e = elution volume; V_o = void volume; V_t = total bed volume of column (25).

Circular Dichroism Spectral Studies—All of the far UV CD spectra of HABP1 were recorded on a JASCO 715 spectropolarimeter in the buffer of different pH values. The scans were taken between 250 and 200 nm at 10 °C. The samples were prepared 4–24 h before recording the spectra in the desired buffer and filtered through 0.22-μ Millipore membranes. A rectangular cuvette of 1-mm path length was used throughout the experiment. The concentration of protein was kept constant at 10 μM. Data were recorded at a scan speed of 50 nm/min with a response time of 1 s at a bandwidth of 1 nm and accumulated at 0.1-nm step intervals. Typically, 3–5 scans were taken for each sample. The buffer baseline was subtracted in each case.

Thermal denaturation of HABP1 (5 μM) was monitored by change in molar ellipticity at 222 nm with increasing temperature on a JASCO 715 spectropolarimeter, equipped with a Peltier temperature controller (JASCO PTC-348 WI). The wavelength was decided on the basis of the minima of the difference spectra obtained by subtracting the native protein scan from the thermally denatured protein scan. The samples and buffers were prepared as described above. Samples were heated at a constant rate of 60 K h^{-1} and data were accumulated at 0.1-K intervals. Analyses of the data were carried out with Origin version 5.0 using a two-state transition model.

Differential Scanning Calorimetric Studies—All calorimetric scans were performed on the ultrasensitive differential scanning calorimeter, VP-DSC (Microcal Inc.). The protein samples on which DSC scans were performed as a function of salt concentration were prepared in 10 mM phosphate buffer, pH 7.2. The ionic concentration was varied using NaCl. Samples for the pH-dependent scans were prepared in different buffers (phosphate, pH 6.5–8; MES, pH 5.5–6.3; acetate, pH 4.0–5.4) at a fixed ionic concentration of 200 mM. The protein samples were extensively dialyzed against the desired buffer, typically dialysis was done in 1:1000 samples to buffer ratio with 5 changes (1:1000 × 5) at 4 °C. The sample and the last dialysis buffer were filtered and degassed before being scanned in the calorimeter. The 0.5-ml sample was introduced into the sample cell and a similar amount of the last dialysate was introduced into the reference cell and the calorimeter was up-scanned at a constant rate. Protein concentration was determined by measuring *A* at 280 nm as described earlier. The calorimetric unit was interfaced to a microcomputer for automatic data collection and analysis. The best least squares fit of the two-state transition model, $A_3 \Leftrightarrow 3B$, where A is the folded state and B is the unfolded state, to the data were determined

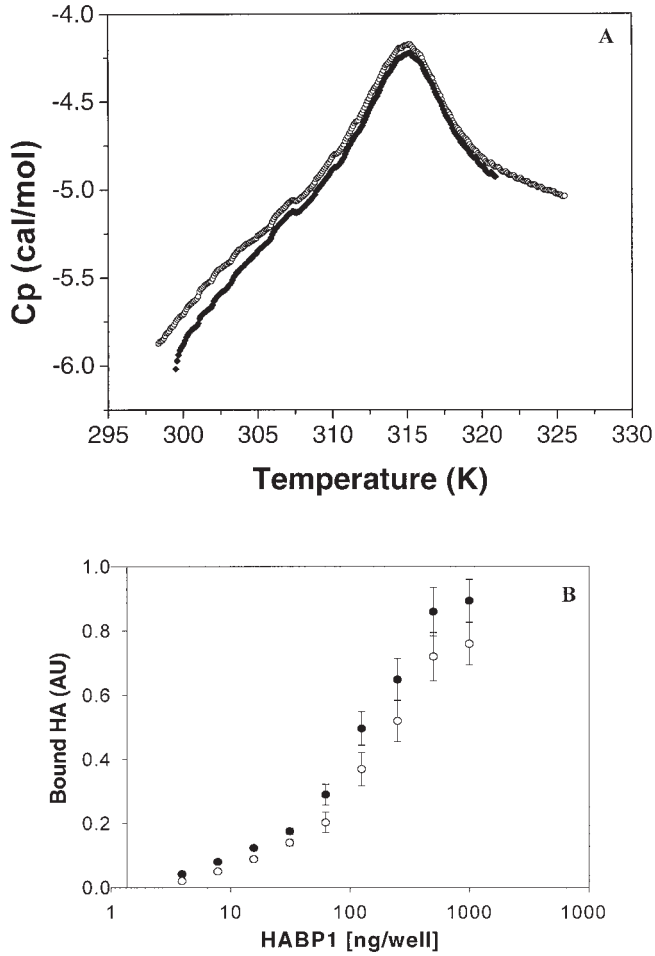

FIG. 3. **Thermodynamic and biochemical reversibility.** HABP1 exhibits perfect thermodynamic as well as biochemical reversibility. *A*, raw data obtained from DSC scans of HABP1 (*open circle*) and rescanning the same protein sample (*closed diamond*). 14 μM HABP1 in 10 mM phosphate-buffered saline (100 mM NaCl) was up-scanned at a heating rate of 20 K h^{-1} beyond its transition midpoint temperature. The same sample was then cooled to 10 °C and up-scanned again. The graph shows the plot of excess C_p *versus* temperature. *B*, microtiter plate-based HA binding assay of native (*solid circle*) and renatured (*open circle*) HABP1 shows perfect biochemical reversibility. For this binding assay 100 μl/well of native and thermally denatured HABP1, renatured by slow cooling, were coated in a 96-well enzyme-linked immunosorbent assay plate in triplicates as described under "Materials and Methods" and incubated with biotin-labeled HA. The bound HA was detected with 1:10,000 dilution of HRP-conjugated extravidin using ABTS as substrate. Bound HA was plotted against the increasing concentration of HABP1. The S.D. ($n = 3$) is shown as *error bars* on each data point.

using Origin version 5.0 software supplied with the instrument. Analyses of normalized data utilizing the progress base line connection of pre- and post-transition base line of the DSC thermogram yielded the van't Hoff enthalpy (ΔH_v), transition midpoint temperature (T_m, the temperature at half the peak area), and the transition peak area, which when divided by the number of moles of protein in the cell, yields the calorimetric enthalpy (ΔH_c). The ratio of $\Delta H_c/\Delta H_v$ yields the cooperativity of transition (26). All the scans at ionic concentrations of 100 mM NaCl or above were found to be reversible.

Hyaluronan Binding Assays—Microtiter plate binding assays were carried out to investigate the effect of pH on the interactions of HA with HABP1. The assays, which are based on those described previously (22, 27), determine colorimetrically the level of binding of HABP1 to wells coated with HA. All washes were performed in standard assay buffer (SAB: 10 mM phosphate buffer, pH 7.2, containing 150 mM NaCl and 0.05% (v/v) Tween 20). Plastic Costar flat-bottomed high binding microtiter plates (EIA/RIA) were coated (in triplicates) overnight with 100 μl/well of 10 μg/ml HA in 20 mM carbonate buffer ($Na_2CO_3/NaHCO_3$), pH 9.6, at 4 °C. Control wells were treated with buffer alone. The coating solution was removed and the plates were washed three times

TABLE I
Concentration dependence of transition temperature of HABP1
Data were rounded off to first decimal place and error wherever applicable is given in parentheses.

Protein concentration	T_p		T_m	
	200 mM	1000 mM	200 mM	1000 mM
μM	K		K	
	NaCl	NaCl	NaCl	NaCl
3.3	315.0	333.1	315.4 (0.01)	333.1 (0.02)
6.7	315.9	334.4	315.9 (0.03)	334.5 (0.02)
14.0	316.1	335.5	316.1 (0.02)	335.0 (0.01)
27.7	316.9	336.4	317.9 (0.04)	336.0 (0.03)
56.0	317.9	342.0	319.1 (0.05)	341.0 (0.03)

and nonspecific binding sites were blocked by incubation with 1.5% (w/v) bovine serum albumin for 90 min at 37 °C, followed by three washes. Finally, the respective wells were rinsed three times with buffers of different pH values (10 mM sodium acetate, pH 4.0–6.5, and sodium phosphate, pH 6.5–8.5). 100 μl of HABP1 or HABP1-biotin from a 50 μg/ml solution in 10 mM sodium phosphate buffer, pH 6.5–8.5, or acetate buffer, pH 4.0–6.5, containing 150 mM NaCl was added to each well and incubated for 4 h at room temperature or overnight at 4 °C. Plates were washed three times and 100 μl of a 1:10,000 dilution of polyclonal anti-HABP1 antibody (in SAB containing 1% bovine serum albumin) was added and incubated for 90 min, followed by five washes. A 100 μl/well of 1:10,000 dilution of horseradish peroxidase (HRP)-conjugated goat anti-rabbit IgG in SAB containing 1% bovine serum albumin was added to each well and incubated for 1 h at room temperature. For competitive inhibition assays biotinylated HABP1 at different pH values were preincubated with varying concentrations of unlabeled HABP1 and added to HA-coated plates and the bound HABP1-biotin was probed with HRP-conjugated extravidin (1:30,000). The unbound secondary antibodies/extravidin-HRP were sipped out of the wells after 1 h incubation at 37 °C and washed five times and finally rinsed with substrate buffer (100 mM phosphate citrate buffer, pH 5.0). 100 μl of 0.6 mg/ml solution of ABTS in substrate buffer containing 3 μl/ml H_2O_2 was added to each well and incubated for 10 min at 37 °C for color to develop. Absorbance at 405 nm was determined on a microtiter plate reader (Bio-Rad model 550 microplate reader). All absorbance readings were corrected against blank wells.

Solution Binding Assay for HA-HABP1 Interaction—All fluorescence measurements were performed on a LS-55 luminescence spectrometer (PerkinElmer Life Sciences) interfaced with a Multi Temp III (Amersham Biosciences) water circulator to keep the temperature constant. Binding of HA to HABP1 was monitored by adding small aliquots of HA-octa- or polysaccharide to 0.8 μM HABP1 dissolved in a similar buffer at constant temperature. In every case the total volume of aliquots added was always ≤1% of the total reaction volume. A parallel control containing similar disaccharide equivalents of chondritin sulfate A of similar aliquots was run and used as F_0. The fluorescence emission intensity was measured by using an excitation wavelength of 295 nm. For titration experiments, emission was monitored at 350 nm. In every case excitation and emission slit-width of 2.5 and 5 nm, respectively, were used. Fluorescence data were corrected for excitation intensity. Five successive readings with an integration time of 10 s were recorded and averaged value was subtracted from F_0 to get ΔF and plotted against ligand concentration. ΔF_{max} calculated from the plot was further used for the estimation of dissociation constant as reported earlier (28).

Calculation of the Accessible Surface Area Changes upon Trimer Dissociation and Monomer Unfolding—The polar, apolar, and total accessible surface areas (ASA) were calculated with the program Insight, using the methods of Lee and Richards (29). For the folded trimeric HABP1 the coordinates were downloaded (Protein Data Bank code 1ID p32) and analyzed for accessible surface area. The program calculates the atomic accessible surface defined by rolling a spherical probe of a given size around the van der Waals surface. A probe of 1.4-Å radius and a slice thickness of 0.05 Å were used. The output file contained summed atomic ASA over each residue. The ASA of the unfolded protein was calculated as the sum of the accessibility of the residues in an extended Ala-*X*-Ala tripeptide because of the primary structure of the protein. We took the Ala-*X*-Ala surface values from the tripeptide designed in extended conformations for each residue using Insight software.

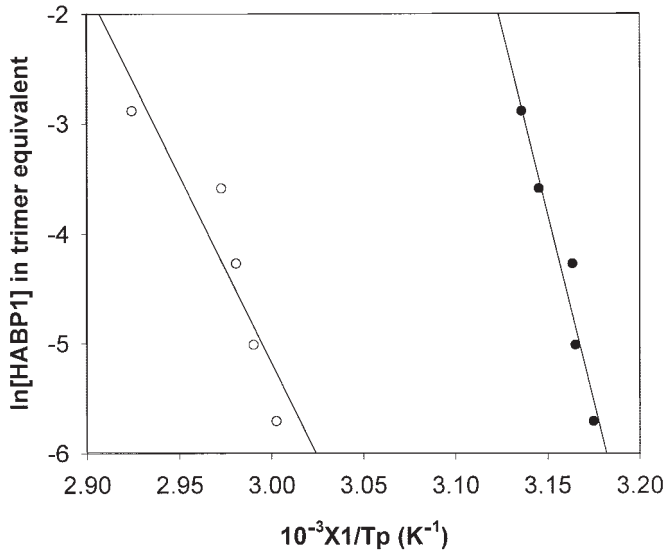

FIG. 4. **Plots of ln [HABP1] against $1/T_p$ for HABP1.** The *lines* are the best least-squares fits of ln [HABP1]/1 mM in trimer equivalent against $1/T_p$ in the presence of 200 mM NaCl (*open circle*) and 1 M NaCl (*solid circle*). The correlation coefficients are 0.96 and 0.98 at 200 mM and 1 M NaCl, respectively. The scan rate was kept constant at 20 K h^{-1} for all concentrations.

TABLE II
Scan rate dependence of T_m at intermediate salt concentration of 200 mM in phosphate-buffered saline
The error in T_m is given in the parentheses.

Scan rate	Tm
Khr^{-1}	K
10	315.6 (0.01)
20	316.1 (0.03)
60	316.0 (0.04)
80	316.2 (0.04)

RESULTS

Hydrodynamic Behavior of Trimeric HABP1 as a Function of pH—To examine if electrostatic repulsion in HABP1, an acidic protein, is indeed responsible for the expanded structure around neutral and basic pH, size exclusion chromatography was carried out as a function of pH keeping the ionic concentration constant. HABP1 showed a gradual decrease in elution volume suggesting a gradual increase in the hydrodynamic volume (V_h) of the molecule with increase in pH (Fig. 1*A*). Therefore, size exclusion chromatographic data were further analyzed for calculating the hydrodynamic size of the molecule by comparing with the standard molecular weight markers of known Stokes radii. The pH-induced structural compaction seems to be the result of reduction in total charges because of de-ionization of various polar amino acid residues, which are

TABLE III
Thermodynamic parameter of HABP1 calculated from a two-state fits as described under "Materials and Methods" with increasing concentrations of salt

Errors have been given in parentheses.

Salt concentration	T_m	ΔH_c	ΔH_v	$\Delta H_c/\Delta H_v$
mM	*K*	*kcal mol*$^{-1}$		
100	306.4 (0.02)	29.7 (0.1)	107.0 (0.4)	0.28
200	315.9 (0.01)	33.7 (0.2)	142.0 (0.7)	0.24
300	321.7 (0.01)	54.1 (0.3)	147.0 (1.0)	0.37
600	330.3 (0.05)	57.6 (0.2)	180.0 (0.9)	0.32
10,000	336.4 (0.04)	70.6 (0.5)	208.9 (3.8)	0.34

asymmetrically distributed on trimeric HABP1. The total charge present on HABP1 at different pH values was calculated using ANTHEPROT and plotted against pH along with the Stokes radius at the corresponding pH (Fig. 1*B*). The total charge on trimeric HABP1 at pH 7.2 is −83 as compared with that of +8.0 at pH 4.0. The important observations of our study are concerned with strikingly different states of compaction of HABP1, induced by pH. For example, HABP1 trimer under alkaline pH is so expanded that it elutes much earlier than the compact trimer. There is a gradual increase in the compactness of trimer with decreasing pH. The decrease is such that the compact form of the trimer has a Stokes radius of 30.7 ± 1.4 Å (n = 3) at pH 4.5 compared with the most expanded trimer, which has a Stokes radius of 40.5 ± 1.5 Å at pH 9.0 (n = 3). All these experiments were performed at a fixed ionic concentration.

Model for Fitting the Differential Scanning Calorimetric Data of HABP1 Unfolding—We have shown previously that the absence of counter ion drastically affects the structure as well as conformation of trimeric HABP1 in solution, which to a great extent seems to be responsible for the generation of binding sites for different ligands under different conditions of ionic strength (22). Thus, the presence of counter ions in its molecular environment is an absolute requirement for HABP1 to exist in any sort of functionally relevant structure/conformation, especially so for its hyaluronan binding capabilities. Consequently, we proposed that the combination of the high net charge asymmetrically distributed along the faces of the molecule and relatively low intrinsic hydrophobicity of HABP1 resulted in its expanded structure around neutral pH in low ionic environment. Addition of counter ions in the molecular environment minimizes the intra-molecular electrostatic repulsion in HABP1 leading to its stable and compact conformations, which is also reflected in its differential affinity toward different types of ligands.

In this study we have, therefore, scrutinized in detail, the conformational stability and folding of HABP1 in a wide range of salt and pH values using ultrasensitive differential scanning calorimeter. A typical endotherm of HABP1 with the details of the mode of curve fitting procedure, notation, and the definition of various thermodynamic parameters determined are illustrated in Fig. 2. HABP1 (14 μM) in 10 mM sodium phosphate-buffered saline, pH 7.2, was filled in the sample cell and the reference cell, containing buffer alone, was up-scanned. The respective baseline-subtracted data (where the baseline was obtained with buffer in both the sample and the reference cells of the calorimeter) were used in each case for analyses (Fig. 2, *a* and *b*). HABP1 showed a perfect thermodynamic as well as biochemical reversibility from 100 mM salt onwards, as shown in Fig. 3, *a* and *b*, respectively. Therefore the data obtained from the DSC measurements were analyzed by a two-state reversible unfolding, *i.e.* unfolding upon dissociation, fitting model.

Effect of Protein Concentration, Scan Rate, Salt, and pH on Thermodynamic Stability of HABP1—It has been demonstrated by using a number of independent techniques that HABP1 is predominantly trimeric under the experimental conditions in this study (22). For oligomeric proteins, the measured (effective) heat effect of unfolding and melting temperature depends on protein concentration. To see such an effect in the case of HABP1, concentration-dependent calorimetric scans were carried out at two rather extremes of salt concentrations (200 mM and 1 M) in 10 mM phosphate buffer, pH 7.2. A concentration range of 3.33 to 56 μM was chosen for the purpose, keeping a scan rate of 20 K h^{-1}. T_p (temperature at which maximum excess heat capacity was seen) increased with increasing protein concentration. This suggested that the dissociation of the HABP1 oligomer occurs during thermal unfold-

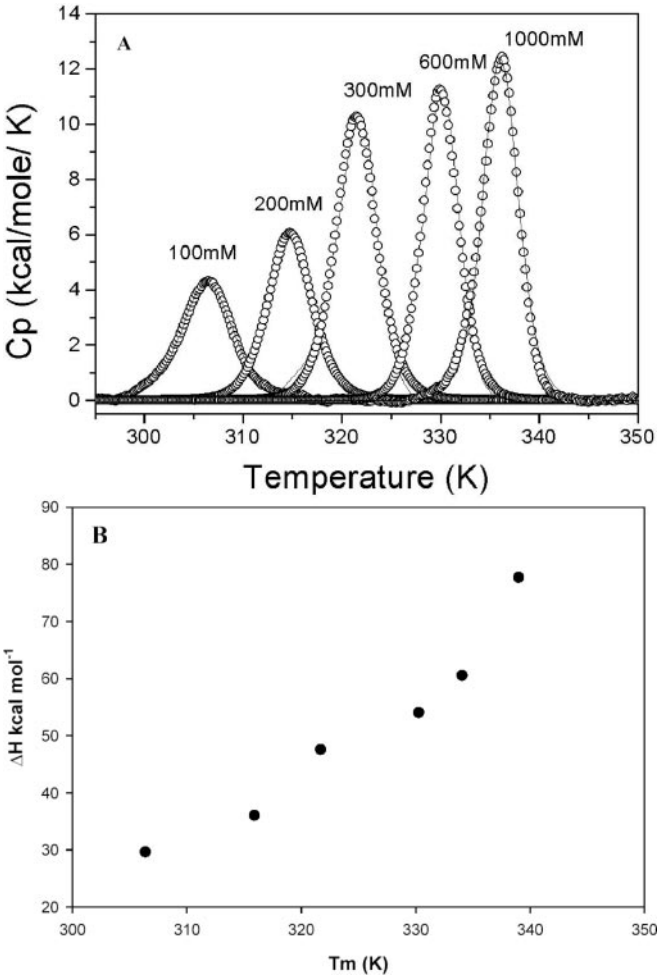

FIG. 5. **Effect of ionic strength on the thermodynamic stability of HABP1.** *A*, plot showing the normalized raw data after processing as described in the legend to Fig. 2 (*open circle*) along with the two-state fit (*solid line*) at different salt concentrations. 14 μM HABP1 in 10 mM phosphate buffer containing different amounts of NaCl, pH 7.2, were up-scanned at a scan rate of 20 K h^{-1}. *B*, plot of enthalpy against T_m with increasing salt concentrations.

TABLE IV
pH dependence of thermodynamic parameter of HABP1 as calculated from analysis of DSC data using two-state fits
An error in each case is given in parentheses.

pH	T_p	T_m	ΔH_c	ΔH_v	$\Delta H_c/\Delta H_v$
	K		*kcal mol*$^{-1}$		
5.0	334.0	333.6 (0.04)	59.5 (0.8)	180.0 (5.4)	0.33
5.5	327.0	327.6 (0.05)	56.3 (0.7)	167.5 (4.7)	0.34
6.0	322.4	322.4 (0.02)	55.5 (0.4)	157.0 (1.51)	0.35
6.6	319.5	319.1 (0.03)	53.8 (0.6)	166.0 (3.7)	0.32
7.0	318.5	318.3 (0.04)	52.8 (0.8)	158.0 (2.8)	0.33
7.2	315.1	314.9 (0.01)	50.1 (0.1)	132.0 (0.7)	0.27
7.5	315.0	313.9 (0.05)	12.0 (0.6)	39.7 (6.5)	0.30
8.0	313.0	313.2 (0.02)	6.4 (0.1)	18.5 (2.6)	0.34

ing, as the ratio of $\Delta H_c/\Delta H_v$ equals 0.3. The data are presented in Table I and shown in Fig. 4, where, ln[HABP1]/1 mM in trimer equivalent was plotted as a function of $1/T_p$ (K^{-1}) at two extremes of salt concentrations. The least-squares fit of a straight line to the data points yields a slope of (-3.404 ± 0.579) $\times 10^4$ K at 200 mM salt concentration and (-6.856 ± 0.408) $\times 10^5$ K at 1 M salt concentration. It has been shown earlier (30–32) that for an oligomer undergoing dissociation, this slope should be,

$$d(\ln[HABP1])/d(1/T_p) = \Delta H_v(S)/\{R(n-1)\} \quad \text{(Eq. 1)}$$

where n is the oligomerization number. For HABP1 where $n = 3.0$, $\Delta H_v(S)$ is the same as ΔH_v for the transition (27, 33) and equal to 136.17 ± 21.8 kcal mol^{-1} at 200 mM and 274 ± 16.44 kcal mol^{-1} at 1 M salt concentration. Because T_p is determined from the raw data and not from the fits using the two-state transition model, the agreement of $\Delta H_v(S)$ with ΔH_v (which is determined from application of the two-state model to the data) constitutes an independent confirmation that not only does the denaturation of HABP1 result in dissociation, but the application of the two-state transition model to the data is justified.

To test any kinetic effect on the thermal unfolding of HABP1, DSC melts were performed at scans rates from 10 to 90 K h^{-1} in 10 mM phosphate buffer containing 200 mM NaCl, pH 7.2. The scan rate dependence of the T_m of HABP1 is given in Table II. The data suggest that the difference in T_m as a function of scan rate is insignificant, and fall well within the instrumental response, hence asserting to the fact that the thermodynamic model used for calculation is correct and the scan rate independent.

It was observed that HABP1 DSC scans did not give any enthalpically relevant transition below 50 mM salt concentration. It was suggested that any enthalpically relevant structural formation in HABP1 starts at 50 mM salt, below which it remains in a molten globule-like state. The enthalpically relevant transition could not be observed in such cases although the molecule may have some degree of intact structure (34). The transition becomes apparent as soon as the ionic strength of the buffer is increased, suggesting a disorder to ordered transition of HABP1 with increasing salt concentration as observed in the case of some other proteins that exist as natively disordered structures (24, 34–38).

The thermal stability of HABP1 increases gradually with increasing ionic strength of the buffer. An appreciable transition is observed at around 50 mM salt with a T_m of 304.52 ± 1.65 K ($n = 3$), which increases linearly until 1 M salt (Table III). A gradual increase in enthalpy was also observed with increasing salt concentration. The raw data (*open circle*) after the buffer baseline correction along with the two-state fit (*solid line*) at different salt concentrations (indicated on the *top* of each *curve*) are illustrated in Fig. 5*A*. Increase in T_m along with ΔH itself gives a fair indication of the structural stability of HABP1 with increasing salt concentrations (Fig. 5*B*).

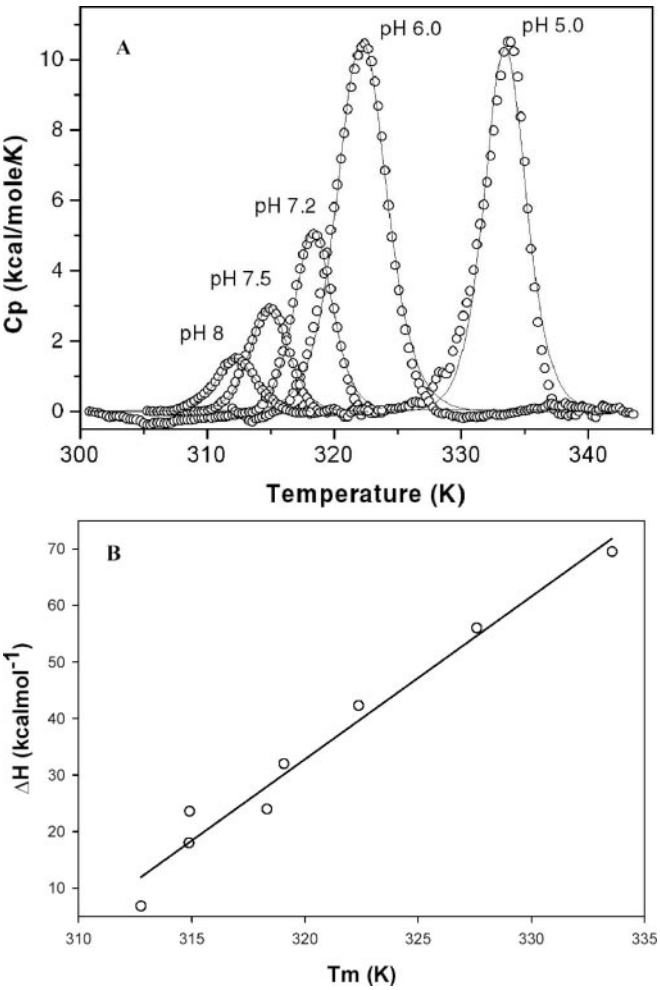

FIG. 6. **Effect of pH on the thermodynamic stability of HABP1.** *A*, plot showing the normalized raw data after processing as described in the legend to Fig. 3 (*open circle*) along with the two-state fit (*solid line*) at different pH values keeping the ionic strength fixed at 200 mM NaCl. 14 μM HABP1 in 10 mM buffers of different pH (phosphate, pH 6.5–8; MES, pH 5.5–6.3; acetate, pH 4.0 5.4) were up-scanned at a scan rate of 60 K h^{-1}. *B*, plot of T_m against the change in enthalpy as a function of pH. Slope of this line yielded the ΔC_p.

The ratio $\Delta H_c/\Delta H_v \approx 0.32$ (±0.03) is constant at 100 mM and higher salt concentrations (Tables III and IV). This is indicative of the fact that three independent unfolding units exist in the HABP1, which may be identified as the three subunits of the molecule. Thus, the completely denatured HABP1 exists as a monomer, whereas in the native state it exists as a trimer.

HABP1 is an acidic protein (pI = 4.1) with asymmetric charge distribution along the faces including propeller-like channels of the molecule. Electrostatic repulsion is thought to be the major destabilizing force in the absence of counter ions.

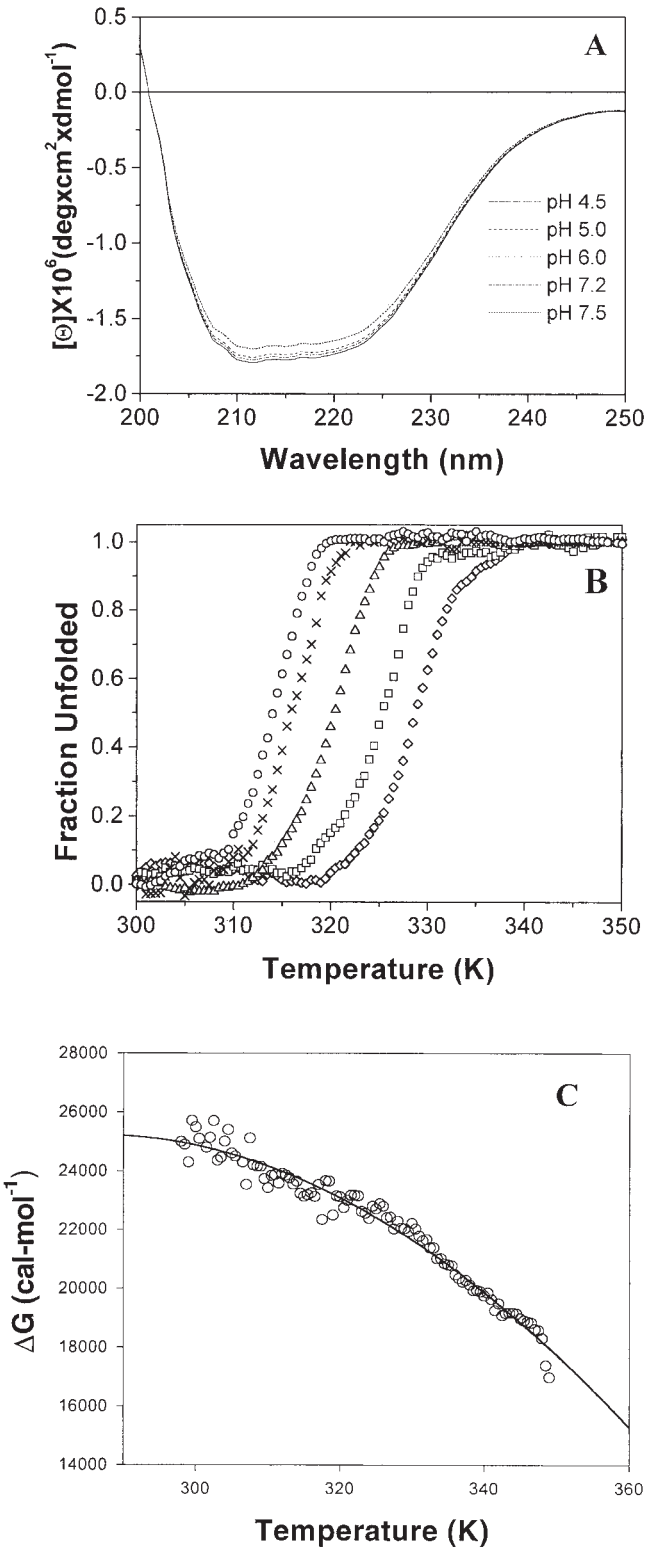

FIG. 7. **Thermal denaturation of HABP1 as observed from measuring the change in molar ellipticity.** *A*, representative CD spectra of HABP1 in the buffer of different pH values at fixed ion concentrations. The protein concentration was kept at 10 μM in terms of HABP1 monomer. *B*, plot of the fraction of protein unfolded with increasing temperatures. Different curves represent temperature melts of HABP1 at different pH values, 8 (○), 7.2 (×), 6.8 (△), 6.4 (□), and 5.0 (◇). *C*, plot of free energy with increasing temperatures.

Our data on the pH-induced compaction of the hydrodynamic volume of HABP1 also supports these interpretations. To examine the thermodynamic stability of HABP1 as a function of pH we investigated the effect of pH on the stability of HABP1. HABP1 in the presence of 200 mM NaCl in 10 mM buffer ranging from pH 5 to 8 (sodium phosphate, pH 8–6.5; MES, pH 6.3–5.5; acetate, pH 5.0) were analyzed. The concentration of HABP1 was kept constant at 14 μM at all pH values.

TABLE V
Thermodynamic parameter of HABP1 calculated from a two-state fit as described under "Materials and Methods" with increasing concentration of salt using CD thermal melt

Errors in each case are given in parentheses.

Salt concentration	T_m	ΔH_v
mM	*K*	*kcal mol^{-1}*
100	309.0 (0.8)	115 (±16)
200	316.0 (0.7)	154 (±28)
300	321.0 (1.0)	158 (±19)
600	335.0 (1.2)	210 (±25)
10,000	341.0 (1.1)	218 (±22)

TABLE VI
pH dependence of various thermodynamic parameter of HABP1 as calculated from CD thermal melt

pH	T_m	ΔH_v
	K	*kcal mol^{-1}*
5.0	345.0 (1.1)	225 (±28)
5.5	351.0 (1.5)	210 (±18)
6.0	334.0 (0.8)	185 (±29)
6.6	328.0 (0.9)	172 (±15)
7.0	321.0 (1.2)	147 (±33)
7.2	314.0 (1.3)	132 (±29)
7.5	313.0 (0.6)	48.5 (±22)

The raw data were processed as described earlier and the representative curves are shown in Fig. 6*A* along with the fit. The results of the fits of the data are given in Table IV. It is evident from the data that HABP1 is more stable under acidic pH conditions. The transition midpoint temperature at pH 8.0 is 40.18 ± 0.96 °C with a very small value of ΔH_c of 6.38 ± 0.68 kcal mol^{-1} compared with values of 60.57 ± 0.65 °C with a ΔH_c of 59.5 ± 0.983 kcal mol^{-1} at pH 5.0. This large shift in the transition midpoint temperature is expected because of the fact that the electrostatic repulsive force in HABP1 seems to be a major source of its destabilization. At lower pH values the negatively charged amino acid residues are protonated allowing the protein to fold in a more compact fashion.

Thermodynamic Parameters Using CD Thermal Melt—HABP1 exhibited a CD spectrum typical of $\alpha + \beta$ class of proteins with double minima at 220 and 210 nm in the pH range 4.5–8.5 (Fig. 7*A*). HABP1, 7.0 μM, in trimer equivalents under different conditions of pH and ionic strength were heated at 60 K h^{-1} and the molar ellipticity was monitored at 220 nm (a minimum of the difference spectra of native and thermally denatured HABP1) and plotted against temperature (Fig. 7*B*). Analysis of CD thermal melt data were made as described for another trimeric protein considering the unfolding upon dissociation (39). Thus the unfolding equilibrium can be expressed as,

$$F_3 = 3U \qquad \text{(Eq. 2)}$$

where F_3 is the folded trimer and U is unfolded monomer. The equilibrium constant for the above reaction can be written as,

$$K_d = (27\ P_t^2 F_D^3)/(1 - F_D) \qquad \text{(Eq. 3)}$$

where F_D is the fraction of the protein in denatured and dissociated states and P_t is the molar concentration expressed in trimer equivalents. Many physical parameters (y) of the protein solution are related to the fraction of denatured protein by the following equation,

TABLE VII
Accessible surface area changes (ΔASA) for the formation of native HABP1 from unfolded monomers

	Monomer folding		Association		Folding + association	
	Absolute	Relative	Absolute	Relative	Absolute	Relative
	Å²	%	Å²	%	Å²	%
Apolar	6,803	55	2,118	65	8,651	31
Polar	5,499	45	1,125	35	18,880	69
Total	12,302	100	3,243	100	27,531	100

$$(Y_D - y)/(Y_U - Y_F) = (y_U + m_U[T] - y)/(y_U + m_U[T] - (y_F + m_F[T])) \quad \text{(Eq. 4)}$$

where y_F and y_U are y intercepts of the folded and unfolded baselines, respectively, m_F and m_U are the slopes of the folded and unfolded baselines, and T is the temperature (T). The fraction unfolded was plotted against temperature at different pH values (Fig. 7*C*). Substituting the value of F_D in Equation 4, and using,

$$\Delta G = -2.303\mathrm{RT}\log K_D \quad \text{(Eq. 5)}$$

a curve of the dependence of ΔG on temperature were obtained and fitted into a modified form of the Gibbs-Helmholtz equation for trimeric protein derived elsewhere (39).

$$\Delta G_{\text{trimer}} = -R \cdot T\ln(27/4 \cdot P_t^2) + \Delta H_m \cdot (1 - T/T_m) + \Delta C_p \cdot (T - T_m - T \cdot \ln T/T_m) \quad \text{(Eq. 6)}$$

Where R is the universal gas constant, P_t is the concentration in trimer equivalent, T_m is the temperature in Kelvin where F_D is 0.5, ΔH_m is the enthalpy of transition at T_m, and ΔC_p is the change in heat capacity. ΔG *versus* T plot was fitted into the modified Gibbs-Helmholtz equation for the trimeric protein to obtain ΔH_m, ΔC_p, and T_m. A representative fit curve along with the raw data are presented in Fig. 7 and the thermodynamic parameter obtained from the above fitting is presented in Tables V and VI. The inverted parabolic shape of the curve suggests the existence of a low temperature analog of denaturation. Various thermodynamic parameters obtained from the CD experiments are in agreement with those obtained from the calorimetric data. These data support the fact that HABP1 exist as a more compact trimer under acidic pH or in a high ionic strength environment.

Change in ΔASA upon Folding and Trimer Formation—For the ASA calculation the crystal structure of HABP1 (Protein Data Bank code 1P32) was used. Based on this structure, the Lee and Richards (29) method was used for accessibility calculation and the surface area of HABP1 trimer is presented in Table VII.

To obtain the accessible surface area change upon folding a monomeric unit of HABP1,

$$\Delta\mathrm{ASA}_{\text{monomer; folding}} = \mathrm{ASA}_{\text{free monomer; unfolded}} - \mathrm{ASA}_{\text{free monomer; folded}} \quad \text{(Eq. 7)}$$

we calculated first the accessible surface of the unfolded protein $\mathrm{ASA}_{\text{free monomer, unfolded}}$. For this purpose, the accessible surface areas of the residues in a disordered/extended Ala-*X*-Ala tripeptide were multiplied by the number of their occurrences in the polypeptide chain and then totaled (39). To calculate the accessible surface area change per monomer upon trimerization, the following equation was used.

$$\Delta\mathrm{ASA}_{\text{monomer; association}} = \mathrm{ASA}_{\text{free monomer; folded}} - \mathrm{ASA}_{\text{trimerized monomer}} \quad \text{(Eq. 8)}$$

We also intended to obtain the accessible surface area of the monomer that is associated with two other monomers in a trimer, $\mathrm{ASA}_{\text{trimerized monomer}}$. The results reveal that 88% of the surface is buried upon folding of the monomers. For trimerization, the portion of the polar surface change and apolar surface change are 81 and 72%, respectively, upon folding. A high ratio of polar contacts in the subunit interactions of some other proteins has recently been observed (40). Using the change in surface area of monomer upon folding and trimerization, the theoretical ΔC_p was calculated using Equation 9, according to Ref. 41 as the following equation.

$$\Delta C_p = 0.45(\Delta\mathrm{ASA})_{\text{apolar}} - 0.26(\Delta\mathrm{ASA}_{\text{polar}}) \quad \text{(Eq. 9)}$$

Putting the values of $(\Delta\mathrm{ASA})_{\text{polar}} = 18859.941$ Å² and $(\Delta\mathrm{ASA})_{\text{apolar}} = 44601.3$ Å² the ΔC_p was computed to be 3.5 kcal mol^{-1} K^{-1}, which is in close agreement with the experimentally observed value of 2.87 ± 0.6 kcal mol^{-1} K^{-1} at pH 7.2 in a 200 mM ionic concentration buffer.

Functional Implication of pH-induced Structural Changes in HABP1—HABP1 binds hyaluronan specifically with high affinity (7–9, 19, 22). It has been reported on the basis of a number of experiments, which included the binding of HABP1 with radiolabeled HA (7–9), biotinylated HA (19, 22), and competitive inhibition assays (22). In the present study we have examined whether the pH-induced structural changes in HABP1 can affect the affinity of HABP1 toward its ligand HA. The bindings were performed using the solid phase as well as in-solution binding assays using intrinsic fluorescence at different pH values and temperatures. The data obtained from the solid phase binding assay on HA-coated plates demonstrated that there is either no binding or very little binding of HABP1 with HA below pH 4 or above pH 8.5 (Fig. 8*A*). To see whether these interactions are specific at different pH values, HA-coated plates were incubated with biotinylated HABP1 in the presence of unlabeled HABP1 at different pH values and the bond of HABP1-biotin was plotted with increasing concentrations of unlabeled HABP1 (Fig. 8*B*). The data suggested that these interactions are specific as unlabeled HABP1 compete with biotin-labeled HABP1 at different pH values. There is an increase in HA binding with decreasing pH with maximum binding around pH 5.0. A significant increase in binding at pH 5.0 was observed presumably because of the more compact structure of HABP1. In addition to the compact structure of HABP1 at this pH, it also has very little negative charges. The electrostatic repulsion may be one of the factors limiting HABP1 binding to HA in the alkaline pH range.

In addition, the effect of pH on HA-HABP1 interactions was also analyzed by the in-solution binding assay using fluorometric titration as described under "Materials and Methods." Because each trimeric assembly of HABP1 has nine tryptophans spread all over the molecule therefore, change in fluorescence emission spectra was used as probe for the HA-HABP1 interactions. The fluorescence emission spectra of HABP1 show a maximum at 353 nm when excited at 295 nm, which upon binding to HA shift to 350 nm with reduced emission intensity (Fig. 8*C*). An added advantage of this kind of binding assay was the fact that HA neither absorbs nor emits light in the wavelength region of 295–360 nm (*curve 4*, Fig. 8*C*). The relative fluorescence was plotted with increasing concentrations of HA

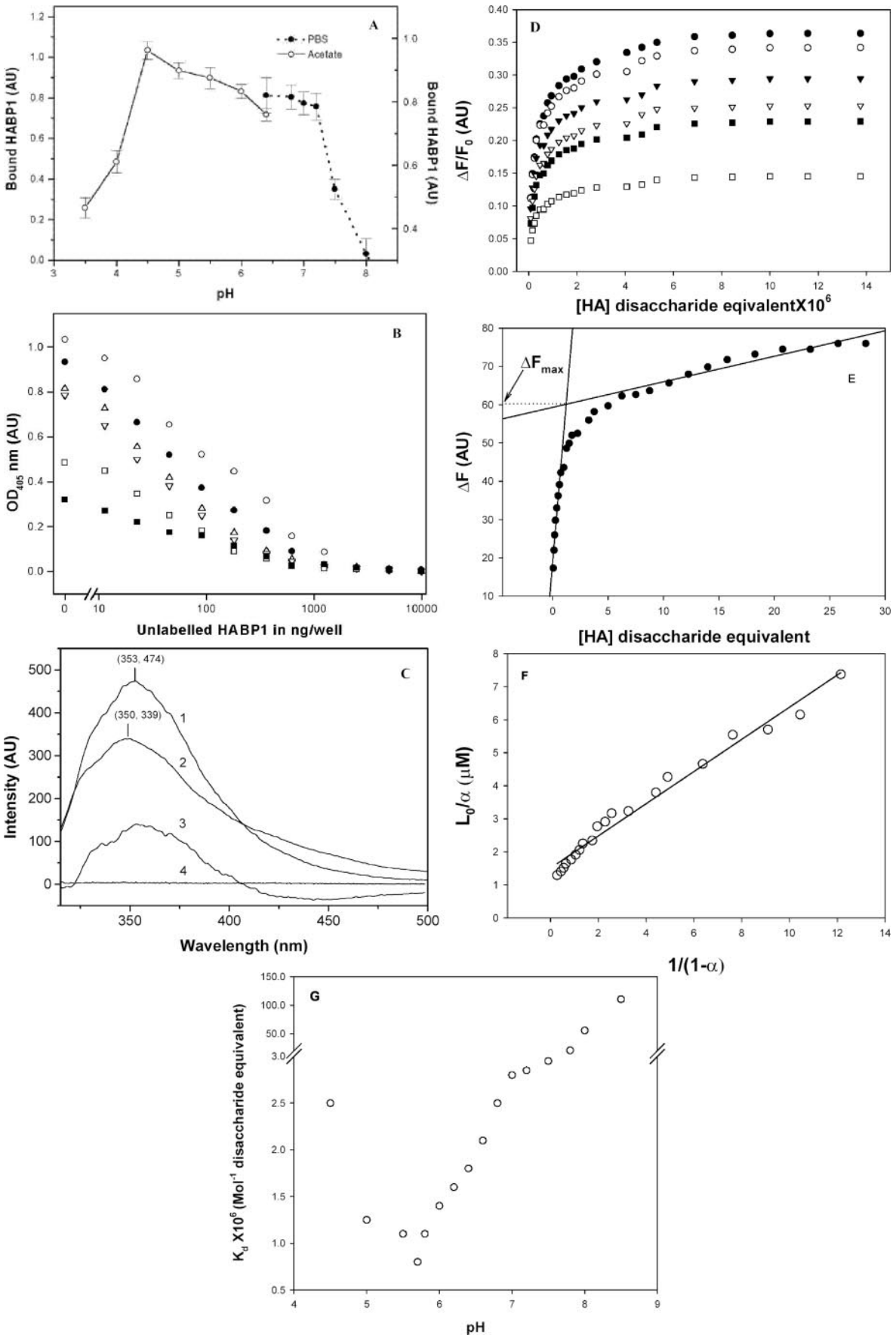

FIG. 8. **Effect of pH on HA-HABP1 interactions.** *A*, HA-coated 96-well assay plates (high binding Costar, EIA-RIA) were incubated with HABP1 in the buffer at different pH values (pH 8.0–6.5 for phosphate and pH 6.4–3.5 for acetate). After removing the unbound HABP1 the bound HABP1 was probed with polyclonal anti-HABP1 antibodies (1:6000) in 10 mM phosphate-buffered saline (PBS), pH 7.2, after washing with PBS containing 0.05% Tween 20 followed by rinsing with PBS. The bound HABP1 at different pH values in arbitrary units are plotted against the pH.

TABLE VIII
Effect of temperature on HA-HABP1 interaction

0.8 μM HABP1 was titrated fluorimetrically by adding small aliquots of 2 mM HA_8 as described under "Materials and Methods" and the data were analyzed as discussed under "Results" at pH 7.2 in phosphate-buffered saline.

Temperature	$K_d \times 10^6$	Number of binding site/mole of HABP1
°C	M^{-1}	
5	25.986	2.9
10	20.265	2.8
15	15.254	3.1
20	10.865	3.1
25	5.865	3.0
30	2.540	3.0
35	15.380	2.7

in disaccharide equivalents and presented in Fig. 8*D*. The data obtained from fluorimetric titration were analyzed using the following standard equation derived elsewhere (28),

$$L_0/\alpha = K_d/(1 - \alpha) + e_0 \quad \text{(Eq. 10)}$$

where L_0 is the total ligand concentration, e_0 is the total concentration of ligand binding site, and α is the fraction of ligand bound at any given ligand concentration, which is defined as $\Delta F/\Delta F_{max}$, ΔF is the change in fluorescence emission intensity at 350 nm and ΔF_{max} was calculated by fitting the linear parts of the L_0 *versus* ΔF curve (Fig. 8*E*). Slope of the plot of L_0/α *versus* $1/(1-\alpha)$ gave the dissociation constant K_d (Fig. 8*F*). In every case the similar disaccharide equivalent of chondroitin sulfate in a similar volume as that of HA was used as a control and subtracted from the experimental data as described under "Materials and Methods." The change in dissociation constant with increasing pH values is shown in Fig. 8*G*. The colorimetric data was further validated by the fact that the dissociation constant shows a similar pattern with pH as does the direct binding under similar conditions when HA was immobilized (Fig. 8, *A* and *G*). The stoichiometry of binding of HA and HABP1 was calculated using highly purified HA-octasaccharide in similar experiments and found to be around 3 in each case. A temperature dependence of HA-HABP1 binding was studied by fluorimetric titration at pH 7.2 and the K_d values at different temperatures are given in Table VIII. The data suggest that for the maximal binding of HA to HABP1 occur at 30 °C, however, there is a slight change in the dissociation constant above or below this temperature and there was no binding observed above the transition midpoint temperature under similar conditions.

DISCUSSION

Interactions of biomolecules are generally controlled by the dynamic nature of energetically viable conformational ensembles adopted by them under different conditions. Especially proteins that have the ability to recognize a number of different ligands, in principle can be expected to be inherently more flexible as this structural flexibility may play an important role in dynamics of biomolecular recognition by them. HABP1 is an example of such a multiligand recognition protein, which is shown to exist in several states in equilibrium, ranging from a substantially unfolded molten globule-like trimer to trimers with varying extents of compaction to a disulfide bonded dimer of trimers (19, 22). This structural plasticity, in part, explains and provides a rationale for its multifunctional nature. In this study, for the first time, we report the thermodynamic stability of HABP1 as a function of ionic strength and pH and quantify the various forces responsible for the structural transitions involved and finally its implication for hyaluronan affinity.

Increasing counter ions in the molecular environment of HABP1 either by changing ionic strength or by decreasing pH, result in compact HABP1 trimer as evident from the decreased Stokes radius. It is likely that the size compaction in the acidic pH range is because of the abolition of electrostatic repulsion as a result of deionization of negatively charged amino acid residues present in cluster on its surface. These observations are consistent with the theoretical calculations reported here, which demonstrate that unlike most globular proteins, the ΔASA of polar amino acid upon folding (81%) is relatively higher than that of apolar residues (72%) in the case of HABP1. The presence of polar amino acids in the interior of protein probably leads to the instability of protein in the low ionic environment under alkaline pH as suggested in a number of reports (42, 43). However, at acidic pH, deionization of these amino acids abolishes the electrostatic repulsion allowing the protein to fold in a more compact fashion. A similar effect was observed by the surface charge screening with counter ion (22). Thus our data suggest that, in general, both proton and counter ions affect the charge interactions at the surface of HABP1 in a similar fashion. These interpretations are supported by observations on several other proteins that have a high degree of repulsive surface charge density (38, 44–46).

We examined if the ionic strength and pH-induced structural compaction has any effect on thermodynamic stability of HABP1. We observed that the HABP1 oligomer unfolds reversibly because of a two-state unfolding behavior. In other words, the dissociation of oligomer to monomer and the unfolding of the protein occurs simultaneously. It is true with a number of oligomeric proteins where existence of the folded monomers as they exist in the respective oligomer were not observed (39, 42, 47). From our studies on T_m as well as enthalpy of transition of HABP1, it is apparent that either increasing the ionic strength or decreasing the pH results in enhanced thermal stability. Such increased thermodynamic stability may be attributed to the screening of negative charges at higher ionic strength by counter ions or the deionization of polar amino acid residues under acidic pH. Consistency of thermodynamic parameters obtained (such as ΔH_c and T_m) using either the two-state or the model-independent method also supports the fact that HABP1 unfolds via a two-state mechanism. The intrinsic stability of HABP1 as calculated from calorimetric scans was found to be 25 kcal mol^{-1} under standard conditions at pH 7.2. These observations suggest that the ordering effects either because of charge screening or by deionization of acidic amino acid residues results in a compact structure of HABP1 under these conditions. This observation is consistent with the fact that

Standard deviations ($n = 5$) were plotted as error bars on each data point. *B*, competitive inhibition of bound HABP1-biotin with unlabeled HABP1. HA-coated plates were incubated with HABP1-biotin with increasing amounts of unlabeled HABP1 at pH 5.0 (*open circle*), 4.5 (*solid circle*), 6.0 (*up triangle*), 6.5 (*down triangle*), 7.2 (*open square*), and 8.0 (*solid square*). The bound antibodies were detected with goat anti-rabbit IgG-HRP conjugates (1:10,000) and HABP1-biotin with extravidin-HRP conjugate (1:30,000) using ABTS as a substrate. Each data point is the average of five replicates. *C*, solution binding assay for HA-HABP1. Fluorescence emission spectra of native 0.8 μM HABP1 excited at 295 nm in the absence of HA (*curve 1*), in the presence of 23 μM disaccharide equivalent of the HA polysaccharide (*curve 2*) difference of curves 1 and 2 (*curve 3*) and 0.5 mg/ml HA polysaccharide (*curve 4*) in 10 mM phosphate-buffered saline, pH 7.2. *D*, plot of relative fluorescence ($\Delta F/F_0$) with increasing concentrations of HA at different pH values (pH 4.5, *open circle*; pH 5.0, *solid circle*; pH 6.0, *solid down triangle*; pH 6.5, *open down triangle*; pH 7.2, *solid square*; and pH 8.0, *open square*). *E*, representative curve of the data fitting as described under "Materials and Methods" to calculate the ΔF_{max}. *F*, a representative fit of L_0/α *versus* $1/(1-\alpha)$, where α is the fraction bound and defined as $\Delta F/\Delta F_{max}$ to calculate the dissociation constant (K_d). *G*, plot of K_d with increasing pH.

selective ion binding during protein folding causes the loss of entropy because of selective displacement of water. Under such conditions the contribution of enthalpy takes predominance in the protein folding process (43).

We have recently reported using 8-anilino-1-naphthalenesulfonate binding studies that HABP1 exists in a molten globule-like state at low salt concentrations (0 and 20 mM NaCl), the CD spectra in the absence of salt shows a minima at 205 nm suggesting the existence of the random coil structure of HABP1 (22). However, addition of salt (25–300 mM) facilitates the structure formation in HABP1, which is reflected in the gradual increase in its molar ellipticity at 220 nm and the capacity to bind HA (22). In the present study an enthalpically significant structure was detected only at 50 mM and higher salt concentrations, although as shown previously, HA binding occurred even at lower salt concentrations such as 25 mM where no peak was obtained in a DSC experiment. Therefore as proposed earlier, absence of the enthalpically relevant transition may not necessarily be interpreted as a complete loss of structure or the existence of unfolded/denatured protein (34). We should also mention here that the DSC data collected at 50 mM salt was not completely reversible, which prevented us from thermodynamically evaluating the DSC profile.

HABP1 has a large number of uncompensated charges (48 negative and 25 positive) and lack of hydrophobic residues (hydropathicity of −0.7) making it a protein of low intrinsic hydrophobicity and high net charge around neutral pH. This protein has specific features such as anomalous migration in SDS-PAGE, high vulnerability to proteolysis, and lack of a secondary structure at low ion concentration (22). All these characteristics are reminiscent of "intrinsically unstructured proteins" (24, 36, 48–51). Therefore, we analyzed the amino acid frequencies in HABP1 and compared them with that in ordered (SwisPROT and globular proteins) and intrinsically unstructured proteins (24, 36, 48–51). According to reports, Pro, Glu/Asp, Lys, Ser, and Gln are termed as disorder promoting and Trp, Tyr, Phe, Cys, Ile, Leu, and Asn are order promoting amino acid residues, whose relative frequencies in polypeptide chains determine their extent of flexibility. HABP1 and intrinsically unstructured proteins almost have similar frequencies of Glu, Lys, Ser, and Tyr, Cys, Ile, and Met. However, frequencies of Asn, His, Leu, and Trp amino acids are comparable with globular or SwisProt™ proteins. Experimental observations along with the similarity in the amino acids distribution indicate that HABP1 in low salt or above neutral pH behaves like an intrinsically unstructured protein.

HA, an important constituent of extracellular matrix having diverse roles in regulating various cellular processes shows a high degree of pH dependence in its interactions with HABP1. In-solution binding assays have demonstrated beyond any doubt that the structural changes in HABP1 induced by either change in ion concentration or pH affect its binding capacity toward HA. Each HABP1 trimer can bind three HA_8 suggesting the presence of three HA-binding sites on each trimeric assembly. TSG6 another important member of the hyaladherin family also shows qualitatively similar behavior in its interaction with HA, because it has maximum affinity to HA under acidic pH conditions (27). Thus, intracellular pH changes that occur in bacterial and viral infection may regulate HABP1 interaction to HA. Thus, the high degree of structural flexibility of HABP1 regulated by the microenvironment in terms of pH and ion concentration may affect cellular processes.

In summary, the asymmetric charge distribution along the faces of HABP1 in association with cations and pH in the molecular environment play critical roles in maintaining its physical stability and three-dimensional structure at secondary, tertiary, and quaternary levels in solution. These factors govern its structural transitions from disordered to ordered and regulate its affinity toward HA. Thus, it seems logical to conclude that the electrostatic repulsion, together with an accessible hydrophobic core of HABP1 and the consequent dynamics because of its intrinsic flexibility imparts a repertoire of ligand recognition specificity and biological functions to this protein.

REFERENCES

1. Lee, J. Y., and Spicer A. P. (2000) *Curr. Opin. Cell Biol.* **12,** 581–586
2. Day, A. J., and Prestwich, G. D. (2002) *J. Biol. Chem.* **277,** 4585–4588
3. Turley, E. A., Bourguignon, L., and Noble, P. W. (2002) *J. Biol. Chem.* **277,** 4589–4592
4. Toole, B. P., Wright, T. N., and Tammi, M. I. (2002) *J. Biol. Chem.* **277,** 4593–4596
5. Fraser, J. R. E., and Laurent, T. C. (1996) in *Extracellular Matrix, Molecular Components and Interactions* (Comper, W. D., ed) pp. 141–199, Vol. 2, Harwood Academic Publishers, Amsterdam
6. D'Souza, M., and Datta, K. (1985) *Biochem. Int.* **10,** 43–51
7. Deb, T. B., and Datta, K. (1996) *J. Biol. Chem.* **271,** 2206–2212
8. Gupta, S., Babu, B. R., and Datta, K. (1991) *Eur. J. Cell Biol.* **56,** 58–67
9. Gupta, S., and Datta, K. (1991) *Exp. Cell Res.* **195,** 386–394
10. Ranganathan S., Ganguly, A. K., and Datta, K. (1994) *Mol. Reprod. Dev.* **38,** 69–76
11. Ranganathan, S., Bharadwaj, A., and Datta, K. (1995) *Cell. Mol. Biol. Res.* **41,** 467–476
12. Krainer, A. R., Mayeda, A., Kozak, D., and Binns, G. (1991) *Cell* **66,** 383–393
13. Ghebrehiwet, B., Lim, B. L., Peerschke, E. I., Willis, A. C., and Reid, K. B. (1994) *J. Exp. Med.* **179,** 1809–1821
14. Ghebrehiwet, B., and Peerschke, E. I. (1998) *Immunobiology* **199,** 225–238
15. Ghebrehiwet, B., Jesty, J., and Peerschke, E. I. (2002) *Immunobiology* **205,** 421–432
16. Ghebrehiwet, B., Lim, B. L., Kumar, R., Feng, X., and Peerschke, E. I. (2001) *Immunol. Rev.* **180,** 65–77
17. Soltys, B. J., Kang, D., and Gupta, R. S. (2000) *Histochem. Cell Biol.* **114,** 245–255
18. Jiang, J., Zhang, Y., Krainer, A. R., and Xu, R. M. (1999) *Proc. Natl. Acad. Sci. U. S. A.* **96,** 3572–3577
19. Jha, B. K., Salunke, D. M., and Datta, K. (2002) *Eur. J. Biochem.* **269,** 298–306
20. Pace, C. N. (1995) *Methods Enzymol.* **259,** 538–544
21. Saunders, A. J., Davis-Searles, P. R., Allen, D. L., Pielak, G. J., and Erie, D. A. (2000) *Biopolymers* **53,** 293–307
22. Jha, B. K., Salunke, D. M., and Datta, K. (2003) *J. Biol. Chem.* **278,** 27464–27472
23. Goto, Y., Calciano, L. J., and Fink, A. L. (1990) *Proc. Natl. Acad. Sci. U. S. A.* **87,** 573–577
24. Uversky, V. N., Gillespie, J. R., and Fink, A. L. (2000) *Proteins* **41,** 415–427
25. Siegel, L. M., and Monty, K. J. (1966) *Biochim. Biophys. Acta* **112,** 346–362
26. Swaminathan, C. P., Surolia, N., and Surolia, A. (1998) *J. Am. Chem. Soc.* **120,** 5153–5159
27. Parkar, A., Kahmanna, J. D., Howatb, S. L., Baylissb, M. T., and Day, A. J. (1998) *FEBS Lett.* **428,** 171–176
28. Bagshaw, C. R., and Harris, D. A. (1988) in *Spectrophotometry and Spectrofluorimetry, A Practical Approach* (Harris, D. A., and Bashford, C. L., eds) pp. 91–113, IRL Press Oxford, United Kingdom
29. Lee, B., and Richards, F. M. (1971) *J. Mol. Biol.* **55,** 379–400
30. Fukuda, K., Dan, H., Takayama, M., Kumano, F., Saitoh, M., and Tanaka, S. (1996) *J. Pharmacol. Exp. Ther.* **277,** 1672–1675
31. Marky, L. A., and Breslauer, K. J. (1987) *Biopolymers* **26,** 1601–1620
32. Sturtevant, J. M., Velicelebi, G. J., Aemicke, R., and Lauffer, M. A. (1981) *Biochemistry* **20,** 3792–3800
33. Srinivas, V. R., Reddy, G. B., Ahmad, N., Swaminathan, C. P., Mitra, N., and Surolia, A. (2001) *Biochim. Biophys. Acta* **1527,** 102–111
34. Xie, D., Bhakuni, V., and Freire, E. (1993) *J. Mol. Biol.* **232,** 5–8
35. Jekow, P., Behlke, J., Tichelaar, W., Lurz, R., Regalla, M., Hinrichs, W., and Tavares, P. (1999) *Eur. J. Biochem.* **264,** 724–735
36. Uversky, V. N. (2002) *Eur. J. Biochem.* **269,** 2–12
37. Dyson, H. J., and Wright, P. E. (2002) *Curr. Opin. Struct. Biol.* **12,** 54–60
38. Apetri, A. C., and Surewicz, W. K. (2003) *J. Biol. Chem.* **278,** 22187–22192
39. Backmann, J., Schafer, G., Wyns, L., and Bonisch, H. (1998) *J. Mol. Biol.* **284,** 817–833
40. Salminen, T., Teplyakov, A., Kankare, J., Cooperman, B. S., Lahti, R., and Goldman, A. (1996) *Protein Sci.* **5,** 1014–1025
41. McCrary, B. S., Edmondson, S. P., and Shriver, J. W. (1996) *J. Mol. Biol.* **264,** 784–805
42. Jaenicke, R., and Lilie, H. (2000) *Adv. Protein Chem.* **53,** 329–401
43. Makhatadze, G. I., and Privalov, P. L. (1995) *Adv. Protein Chem.* **47,** 307–425
44. Freire, E., and Biltonen, R. L. (1978) *Biopolymers* **17,** 1257–1272
45. Lommer, B. S., and Luo, M. (2002) *J. Biol. Chem.* **277,** 7108–7117
46. Nishimura, C., Uversky, V. N., and Fink, A. L. (2001) *Biochemistry* **40,** 2113–2128
47. Gittelman, M. S., and Matthews, C. R. (1990) *Biochemistry* **29,** 7011–7020
48. Li, X., Romero, P., Rani, M., Dunker, A. K., and Obradovic, Z. (1999) *Genome Inform.* **10,** 30–40
49. Li, X., Obradovic, Z., Brown, C. J., Garner, E. C., and Dunker, A. K. (2000) *Genome Inform.* **11,** 172–184
50. Romero, P., Obradovic, Z., Li, X., Garner, E. C., Brown, C. J., and Dunker, A. K. (2001) *Proteins* **42,** 38–48
51. Tompa, P. (2002) *Trends Biochem. Sc.* **27,** 527–533